Nanoscale

PAPER

View Article Online
View Journal | View Issue

Cite this: *Nanoscale*, 2025, **17**, 17265

Cost-efficient folding of functionalized DNA origami nanostructures *via* staple recycling†

Emilia Tomm, Guido Grundmeier and Adrian Keller *

DNA origami nanostructures are powerful molecular tools for the controlled arrangement of functional molecules and thus have important applications in biomedicine, sensing, and materials science. The fabrication of DNA origami nanostructures commonly requires a high excess of staple strands, leading to material waste and high costs, especially when large numbers of modified staples are to be incorporated. Here, we present a method for recycling non-modified as well as biotinylated and fluorophore-modified excess staple strands using molecular weight cut-off (MWCO) ultrafiltration and reusing them in subsequent folding reactions. The structural integrity of the folded DNA origami nanostructures as well as the incorporation and functionality of the introduced modifications are maintained over at least five folding cycles. The resulting reduction in staple costs due to staple recycling reaches 33% over five folding cycles, with a theoretical maximum of 41% for large numbers of cycles. This cost-effective and sustainable approach is straightforward to implement in any given DNA origami fabrication pipeline and particularly attractive for applications requiring large numbers of expensive modifications where substantial reductions in absolute costs can be achieved in this way.

Received 9th April 2025,
Accepted 3rd July 2025

DOI: 10.1039/d5nr01435b

rsc.li/nanoscale

Introduction

DNA origami nanostructures (DONs) are constructed by folding a long single-stranded scaffold with a set of synthetic oligonucleotides, so-called staple strands, enabling the formation of nanoscale structures with high spatial precision.[1,2] The programmability of DONs allows for the precise positioning of functional molecules, including fluorophores,[3–6] nanoparticles,[7,8] and biomolecules such as proteins and aptamers.[9,10] This versatility has driven the adoption of DONs in diverse application areas, ranging from drug delivery[11,12] and drug discovery[13,14] to sensing[3,5] and nanoelectronics.[15,16] However, in many of those fields, the comparably high costs of DON assembly limit their general and widespread application.

Standard DON folding protocols employ a 10-fold to 100-fold excess of staple strands relative to the scaffold to maximize DON folding yields. After purification of the folded product, non-incorporated staples are usually discarded, leading to high costs and significant waste of material. While factors such as scaffold routing, staple design, and staple concentration influence folding pathways and efficiency,[17,18] the precise relationships between these parameters remain unclear, and the minimum staple-to-scaffold ratio required for efficient folding of a given DON design needs to be determined by trial and error. As a result, high staple excess remains the standard. These costs are exacerbated when modified staples such as biotinylated or fluorophore-labeled ones are incorporated. The strong biotin–streptavidin (SAv) interaction[19] is frequently used for decorating DONs with functional entities such as carbon nanotubes,[20] quantum dots,[21] and enzymes,[22] and further exploited in diverse applications such as cryptography,[23–25] protein patterning,[26,27] and single-molecule studies.[28,29] However, their high cost restricts their use to a limited number of modifications with most studies employing only a small number of biotinylated staples, with a reported maximum of 29 sites per DON.[21] Similarly, fluorophore-labeled staples find use in sensing and imaging applications,[3,5,6] yet their cost limits the number of attached fluorophores and with that intensity and potential arrangements. While Selnihhin *et al.* demonstrated extensive labeling with 120 modifications,[3] this remains an exception. Given these constraints, a cost-efficient method for recycling and reusing both non-modified and modified staples would be highly beneficial for numerous applications of DONs. Recently, efforts have been made to explore scaffold and staple recycling, reflecting a growing interest in sustainable and cost-efficient production methods.[30,31]

Here, we assess the feasibility of recovering non-incorporated non-modified, biotinylated, and fluorophore-labeled DON

Paderborn University, Technical and Macromolecular Chemistry, Warburger Str. 100, 33098 Paderborn, Germany. E-mail: adrian.keller@uni-paderborn.de

†Electronic supplementary information (ESI) available: Larger AFM images, PAGE gels of recovered staple mixtures, projected DON area distributions, sequences of the modified and non-modified staple strands of the DON rectangle. See DOI: **https://doi.org/10.1039/d5nr01435b**

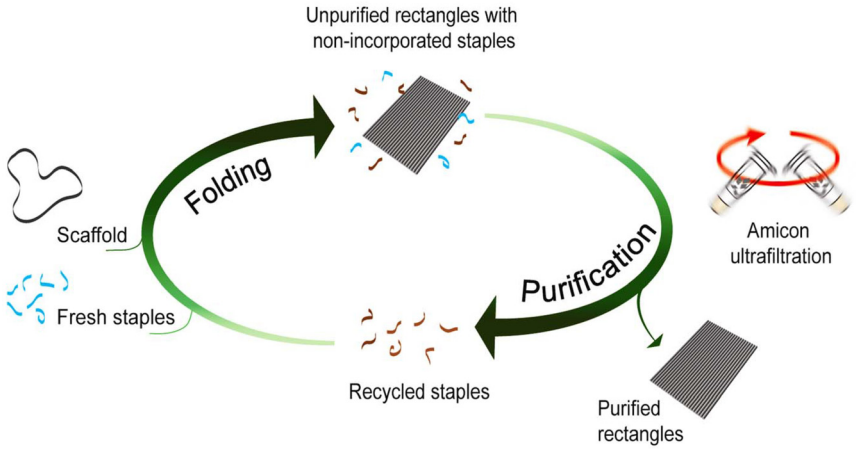

Fig. 1 Schematic representation of the DNA origami staple recycling process. Fresh and recovered staple strands are used to fold DNA origami rectangles, followed by Amicon® ultrafiltration to separate well-folded nanostructures from non-incorporated staples, which are collected and reused in subsequent folding reactions.

staples after folding and reusing them in subsequent folding reactions (Fig. 1). This can be achieved with various purification methods.[32] Polyethylene glycol (PEG) precipitation[33] has recently been used successfully for staple recovery.[30,31] However, residual PEG can interfere with downstream applications, such as agarose gel electrophoresis (AGE).[33–35] To avoid PEG impurities, we thus employed molecular weight cut-off (MWCO) ultrafiltration, which enables efficient staple recovery while minimizing unwanted carryover. The viability of this approach is evaluated over up to 10 consecutive folding cycles. AGE and atomic force microscopy (AFM) reveal successful DON folding from recovered staples without notable impairment of their functionality, thus providing a viable, sustainable, and cost-efficient strategy for DON production.

Results

Minimizing staple excess

A staple excess between 10-fold and 100-fold is widely used in DON assembly, likely due to Rothemund's foundational study demonstrating well-folded structures at these concentrations.[1] However, his experiments also indicated that lower excess down to 2-fold resulted in structurally indistinguishable DONs.[1] While most studies employ higher staple excess to maximize assembly yields, Johnson *et al.* demonstrated that even a 2-fold excess can achieve similarly high yields, provided that annealing temperature is carefully controlled.[36] To determine the minimum excess required for the successful folding of the DON rectangle, we tested DON folding at staple-to-scaffold ratios of 2, 4, 6, 8, and 10. AFM indicates that a 2-fold and, to a lesser extent, 4-fold staple excess results in partially folded and structurally compromised DONs (see Fig. 2a). In contrast, DONs folded at a staple-to-scaffold ratio of 6 and higher appear indistinguishable, suggesting that a 6-fold excess is sufficient to achieve well-formed structures. These observations were further substantiated by AGE. While the electrophoretic mobility of the upper scaffold band remains unchanged, there are some notable differences in intensity (Fig. 2b). In particular, the scaffold/DON bands at 2-fold and 4-fold excess have a higher intensity than at higher excess. This may suggest the presence of partially folded structures that aggregate due to parasitic cross-hybridization of partially incorporated staples. This aggregation is also visible in the AFM images of 2-fold staple excess in Fig. 2a. As staple excess increases, more well-formed DONs assemble, which is accompanied by a higher proportion of non-incorporated staples, resulting in an increased staple band intensity. The similar band patterns observed for 6-fold to 10-fold excess indicate that a 6-fold excess is the minimum required to achieve well-formed rectangular DONs. Therefore, a 6-fold excess was used in all subsequent experiments.

Staple recovery and recycling

To evaluate the feasibility of recycling staple strands and reusing them in subsequent DON folding reactions, we conducted a series of 5 folding and recovery cycles while maintaining a consistent 6-fold excess of staple strands by using non-incorporated staples from the previous cycle step and supplementing with fresh staples (Fig. 1). While removing non-incorporated staples from folded DONs is a standard step, different purification methods exist for separating folded structures from excess staples.[34,37] PEG precipitation, as used in recent studies on scaffold and staple recycling[30,31] has been shown to effectively recover excess staples but residual PEG can influence electrophoretic mobility[34,35] and potentially affect downstream applications. In contrast, we employed MWCO ultrafiltration, which provides a purification strategy that minimizes unwanted carryover. Implementing recycling requires only two additional steps, *i.e.*, measuring the concentration of non-incorporated staples in the filtrate and adding a suitable amount of fresh staples to reestablish the 6-fold staple excess. This was first tested with a non-modified DON rectangle. As

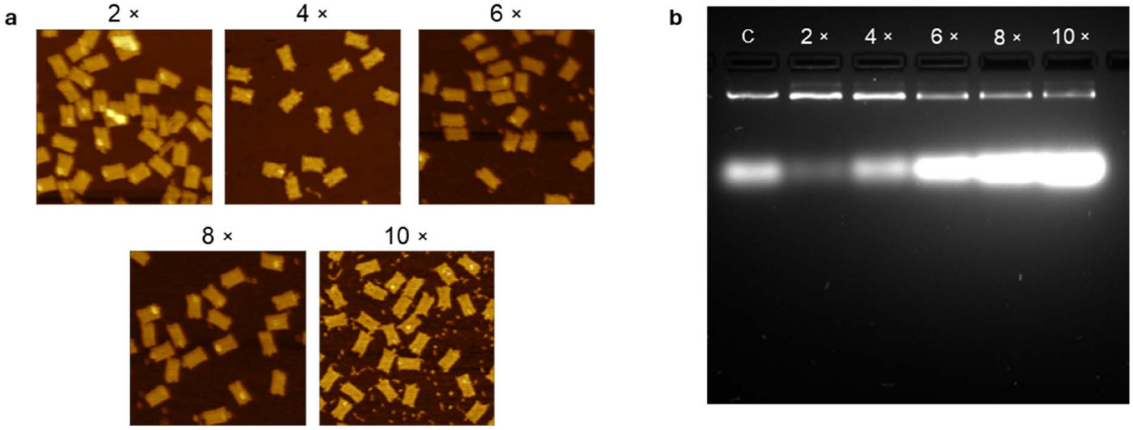

Fig. 2 (a) AFM images (0.75 × 0.75 μm^2) of DON rectangles folded with 2-fold to 10-fold staple excess. Fully formed structures were observed at 6-fold to 10-fold excess, while partial or misfolded structures are visible at 2-fold and 4-fold excess. Height scale for image with 2-fold excess is 11 nm, whereas other height scales are 4.5 nm. (b) AGE image of DONs folded with 2-fold to 10-fold staple excess, alongside a control (C) containing unfolded scaffold and a 4-fold excess of staples. All samples were loaded at a final scaffold concentration of 2.5 nM.

shown in Fig. 3a, the concentration of non-incorporated staples in the filtrate remains rather constant across all 5 cycles, indicating consistent integration of staples during folding. AGE quantification (Fig. 3b and c) reveals that the yields of well-folded DONs and non-incorporated staples remained rather constant over all 5 cycles. Minor intensity variations, such as a slight decrease after step 2 are observed in both bands and are likely due to systematic or experimental errors. Other observations, such as the increased intensity variation between the staple and the DON band observed after steps 4 and 5 may be attributed to variations between individual filters. Nevertheless, these findings demonstrate that the recycling of staple strands can be performed efficiently by MWCO ultrafiltration without compromising folding yield.

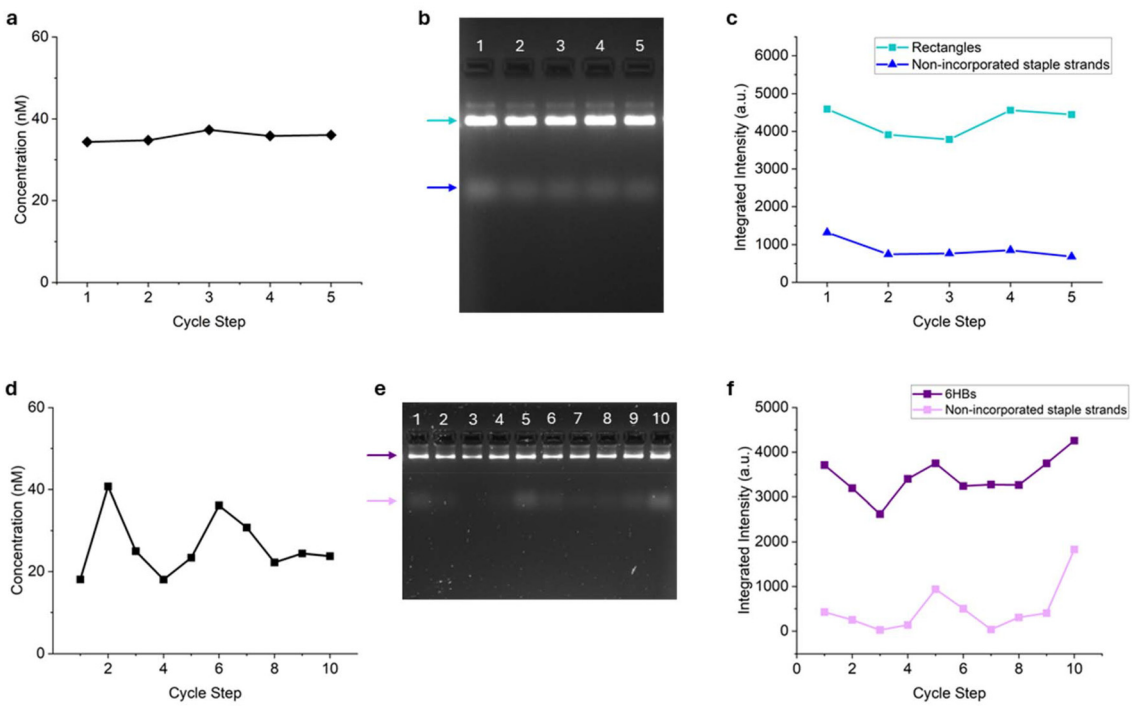

Fig. 3 (a, d) Concentration of non-incorporated staples in the filtrate after each folding and recovery step. A non-modified DON rectangle (a) and a non-modified DON six-helix bundle (6HB) (d) were used, respectively. (b, e) AGE images of folded DON rectangles (b) and 6HBs (e) after 1 to 5 (b) and 1 to 10 (e) full cycles of folding and recovery, respectively. The gels were loaded at a final concentration of 5 nM. (c, f) AGE quantification of DON and staple bands from the gels in b and e, respectively.

We further tested this method over 10 cycles using the same folding, recovery, and recycling parameters but a different DON, *i.e.*, a six-helix bundle (6HB).[21,38] Here, we observed larger variations in the staple concentrations of the filtrate, which can be attributed to variations between individual filters (Fig. 3d). Apparently, the 6HBs with their quasi-1D shape (6 nm diameter, 412 nm length) are more sensitive toward filter variations, presumably because they are able to enter and thereby clog the pores of the filters. Nevertheless, AGE quantification reveals well-folded structures even after 10 cycles (Fig. 3e and f). To evaluate whether such a large number of cycle steps lead to notable staple degradation in the form of fragmentation, the staple mixture recovered after the 10th cycle step was subjected to polyacrylamide gel electrophoresis (PAGE). No notable degradation was observed (Fig. S11†), indicating that the method is compatible with an even larger number of recovery and recycling steps.

Next, we tested this staple recovery and recycling method with a DON rectangle with 5 biotinylated staples. As for the non-modified DON rectangle, the concentrations of non-incorporated staples in the filtrate remained rather constant across all 5 cycle steps (Fig. 4a). Similarly, AGE revealed no major differences in the concentrations of folded biotinylated DON rectangles and non-incorporated staples over the course of recycling (Fig. 4b and c). AFM images of DON rectangles incubated with SAv further reveal relatively constant binding yields across all 5 cycle steps (Fig. 4d and e) ranging from 57% to 71%, which indicates that repeated recycling does not affect the incorporation of biotinylated staples. Furthermore, the preservation of binding capability to SAv confirms that the functionality of biotin modifications remains intact throughout the recycling process. To evaluate the effect of repeated recycling on DON integrity, we quantified the projected DON areas visible in the AFM images. The distributions of the projected areas after recycling steps 1 and 5 reveal that the DONs maintain their average size of around 50 nm^2 (Fig. S12†), suggesting that structural integrity is preserved over multiple recovery and recycling cycles.

Fig. 5 evaluates staple recovery and recycling for a DON rectangle with 3 staples modified with ATTO488 fluorophores. Again, the concentration of non-incorporated staples in the filtrate shows only random fluctuation over 5 recycling cycles. To evaluate the effect of staple recycling on the incorporation of the ATTO488-modified staples, AGE was used. The fluo-

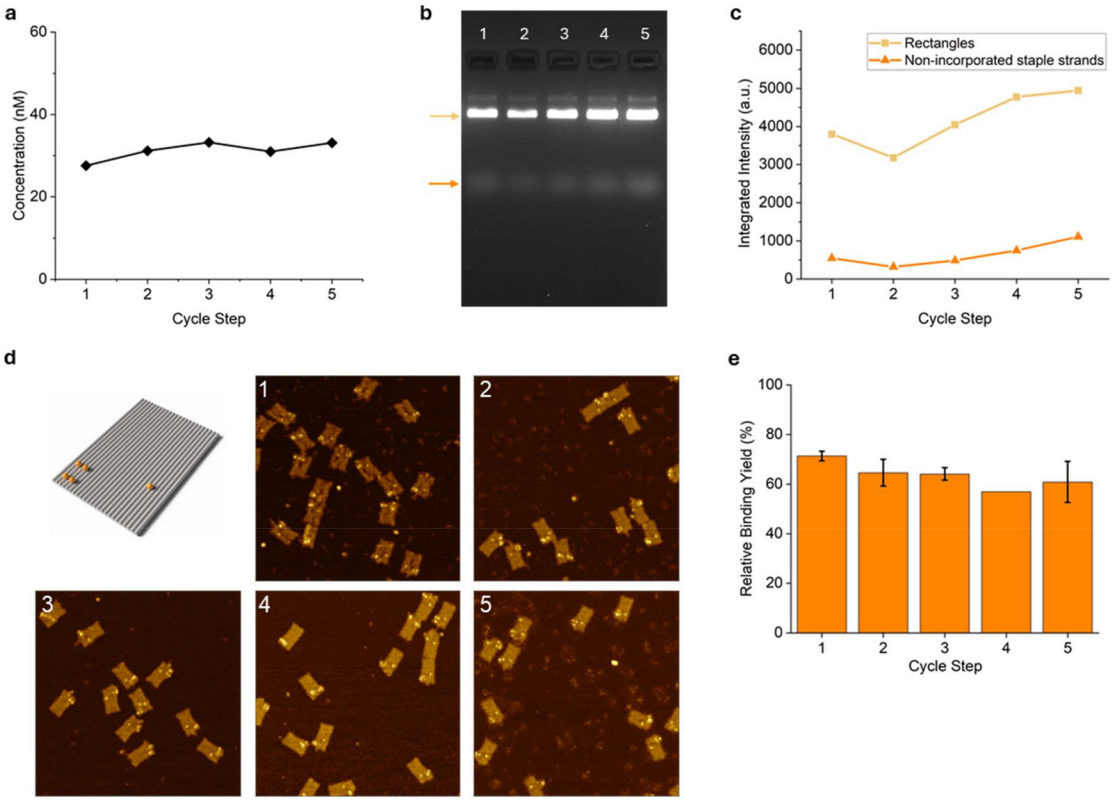

Fig. 4 (a) Concentration of non-incorporated staples in the filtrate after each folding and recovery step. A DON rectangle with 5 biotinylated staples was used. (b) AGE image of folded DON rectangles after 1 to 5 full cycles of folding and recovery, loaded at a final concentration of 5 nM. (c) AGE quantification of DON rectangle and staple strand bands from the gel in b. (d) AFM images (0.75 × 0.75 μm^2) of biotin-modified DON rectangles after each cycle step and subsequent SAv exposure. Height scales are 5.0 nm. The scheme indicates the positions of the 5 biotin modifications. (e) Relative binding yields determined from AFM images. Values are averaged over 2 to 4 AFM images recorded at different positions on the surfaces, corresponding to 288 to 533 DONs. Error bars represent standard deviations. Differences are statistically not significant ($p > 0.05$) as determined by a one-way ANOVA.

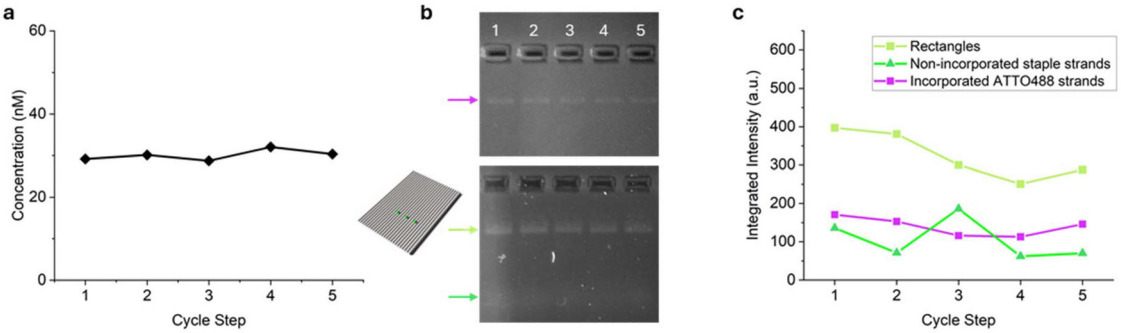

Fig. 5 (a) Concentration of non-incorporated staples in the filtrate after each folding and recovery step. A DON rectangle with 3 ATTO488-modified staples was used. (b) Agarose gel of ATTO488-modified DONs before (upper image) and after post-staining (lower image) with a final DON concentration of 3.2 nM. (c) AGE quantification of ATTO488, DON rectangle, and staple strand bands from the gel in b.

rescence signal of the incorporated ATTO488-modified staples in an unstained gel is localized in a single, well-defined band (indicated by the purple arrow in Fig. 5b) and remains constant across all cycle steps (Fig. 5c). Subsequent staining of the same gel reveals that the ATTO488 fluorescence coincides with the band of the DON rectangles, thus confirming no effect of staple recovery and recycling on incorporation and functionality of the ATTO488-modified staples (light green arrow in Fig. 5b). The intensities of the DON and staple bands show stronger fluctuations than in the previous experiments. This is attributed to the lower overall intensity because of the post-staining applied here, which increases the impact of background fluorescence.

Discussion

Cost efficiency

To evaluate the cost efficiency of the staple recovery and recycling method, we calculated the costs for folding 1 pmol of scaffold (Fig. 6). At current prices (€0.66 per nmol for non-modified, €2.00 per nmol for biotinylated, and €6.18 per nmol for ATTO488-modified staples), folding 1 pmol of scaffold without staple recycling results in staple costs of €0.73 for a non-modified DON rectangle, €0.77 for a DON rectangle with 5 biotinylated staples, and €0.83 for a DON rectangle with 3 ATTO488 modifications. Employing staple recovery and recycling reduces the staple costs with each additional cycle step. After 5 cycle steps, the staple costs are reduced to €0.49, €0.51 and €0.55 per pmol scaffold, respectively, representing an average staple cost reduction of approximately 33.5%. When folding heavily modified DONs with 20 or 100 biotin or ATTO488 modifications, the resulting cost reduction will be substantial (Fig. 6). In large-scale DON production of larger DON amounts, applying more cycle steps will result in further staple cost reductions approaching 41.7% for an infinite number of cycle steps.

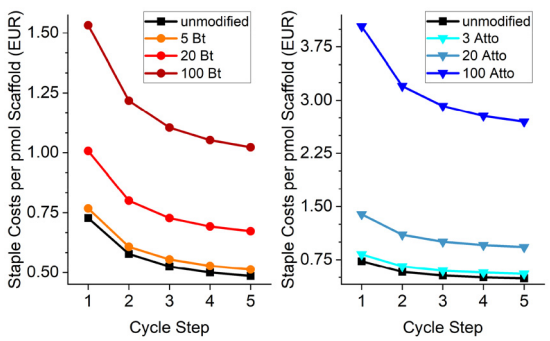

Fig. 6 Staple costs per pmol scaffold for non-modified DON rectangles and DON rectangles with 5, 20 and 100 biotin (Bt) modifications and 3, 20 and 100 ATTO488 (Atto) modifications over the course of 5 cycle steps.

Comparison with PEG-based methods

Both PEG precipitation and MWCO ultrafiltration are effective methods for purifying unmodified DONs, showing comparable yields in standard protocols.[39] In addition, MWCO ultrafiltration has been shown to outperform PEG purification when purifying DONs with small modifications, whereas PEG purification is more suitable for DONs with large protein modifications.[34] However, MWCO ultrafiltration comes with a cost disadvantage. For a 400 µL sample as used in the current study, each purification step with 15% PEG-8000 (w/v) costs approximately €0.023. A single-use 100 kDa Amicon® Ultra filter with a volume of 500 µL costs €4.42. When producing large DON amounts, however, Amicon® Ultra filters with larger volumes can be used. With 15 mL filters, the costs per 400 µL sample could be reduced to €0.42. While this is still substantially more expensive than PEG purification, MWCO ultrafiltration has some additional advantages. In general, PEG purification is more time-consuming and labor-intensive, may leave PEG residues in the sample, and can cause DON aggregation, thereby potentially interfering with downstream processing such as AGE characterization.[30,33–35] Furthermore, recovering the staples from the PEG purification buffer requires an additional ethanol precipitation step.[30,31] This not only adds to the overall effort but may also introduce salt contaminations, which were found to have negative effects on sub-

sequent folding reactions.[31] To solve this issue, multiple ethanol precipitation steps may be necessary, resulting in dramatically increased purification time and labor.[31] In the protocol of Isinelli *et al.*, PEG purification of one sample followed by one round of ethanol precipitation to recover the staples takes about 3 hours and involves multiple steps including freezing the staple supernatant at −80 °C.[31] In contrast, sample purification and staple recovery by MWCO ultrafiltration is straightforward, includes only three rounds of centrifugation in a bench-top centrifuge, and is completed in less than 30 min.

Conclusion

This study demonstrates that the recovery and recycling of non-incorporated staples during DON folding is a viable and effective method to reduce material waste and production costs in DON fabrication. The folding efficiency, structural integrity, and functionality of DON rectangles containing non-modified, biotinylated, and ATTO488-labeled staple strands remain largely unaffected over at least 5 folding cycles. Atomic force microscopy and fluorescence imaging confirm rather constant SAv binding to biotinylated staples and fluorescence from ATTO488-modifed staples, respectively, highlighting the possibility of reusing modified staples without loss of functionality. Furthermore, by employing MWCO ultrafiltration instead of PEG precipitation, our approach ensures high staple recovery while minimizing unwanted PEG residues, making it more suitable for applications that require higher purity.

Our cost analysis further underscores the economic benefits of staple recycling, showing an average cost reduction of about 33% over the course of 5 recycling steps, which becomes particularly relevant for applications requiring large numbers of modified staples. Moreover, extending recycling beyond 5 cycles will yield even greater cost savings up to 41%. In absolute numbers, such cost savings become particularly important when many staple strands with expensive modifications are incorporated, such as the ATTO488 fluorophore employed in the current experiments. This is particularly relevant for various applications such as data storage,[23,40] where the number of modifications per DON directly translates into the storage density, fluorescence-based sensors with high emission intensities,[3] high-throughput drug discovery with DONs presenting many different pharmacophores,[13] and drug delivery with DON vehicles carrying covalently attached drugs.[11]

Finally, we would like to stress that our experiments used established annealing protocols for the selected DON shapes. We only reduced the staple excess from ten-fold to six-fold, while all other parameters, *i.e.*, annealing time, temperature profile, and buffer composition, were kept constant. However, optimizing the annealing protocols by using for instance longer annealing times and more elaborate temperature profiles may allow for further reductions in staple excess and thus further cost savings. Whether this is indeed possible and also economically favorable in view of possibly increased energy consumption and longer synthesis times needs to be investigated in future experiments.

Materials and methods

DNA origami folding and staple recycling

For the preparation of modified rectangular DONs, non-modified staples (Eurofins) were replaced with biotinylated (Eurofins) or ATTO488-modified (Metabion) equivalents (see Table S1†) to achieve an equimolar concentration of each staple strand in the staple stock solution. For staple excess analysis, the DON rectangles were folded using 10 nM scaffold p7249 (100 nM stock, Tilibit) with 2-, 4-, 6-, 8-, and 10-fold staple excess in concentration and 1× TAE (Roth) supplemented with 10 mM $MgCl_2$ (Roth). Folding was performed by heating the mixtures to 80 °C, followed by gradual cooling to room temperature over 90 minutes using a Ristretto Thermocycler (VWR). For the folding of recycling mixtures, a total volume of 400 μL was used, containing 10 nM scaffold p7249 and 60 nM staple strands in 1× TAE with 10 mM $MgCl_2$. The DON 6HBs[21,38] were folded using the same protocol and scaffold with staples purchased from Eurofins.

To separate folded DONs from non-incorporated staples, the solutions were filtered using Amicon® Ultra-0.5 centrifugal filters with a 100 kDa MWCO (Merck). Ultrafiltration was performed at 10 000 rpm for 10 minutes using a MiniSpin® centrifuge (Eppendorf). The DNA concentration in the filtrate was measured with an Implen Nanophotometer P330 (Implen). The first folding step in the recycling cycle served as the initial recycling step, using only fresh staple strands. For recycling steps 2 to 10, 320 μL of the non-incorporated staples recovered from the immediately preceding step were added to the mixture, and fresh staples were used to restore the total staple concentration to 60 nM.

Due to inconsistencies between the manufacturer-specified concentrations of the purchased staple strands (100 μM) and the measured concentrations as determined by UV/Vis absorption, we determined the actual concentrations of all 184 staple strands used for the DON rectangle. Based on their average molecular weight, we then calculated a correction factor, which was subsequently applied to all UV/Vis-based staple concentration measurements, including those of the ATTO488- and biotin-modified rectangles as well as the 6HBs.

Sample recovery and gel electrophoresis

To recover the DONs from the MWCO filters, 350 μL of 1× TAE with 10 mM $MgCl_2$ was added to the filter, followed by centrifugation at 10 000 rpm for 10 minutes. Then, the filters were placed upside down in new filter tubes and centrifuged at 7000 rpm for 7 minutes.

For AGE, the DNA concentrations of the recovered DONs were adjusted to 5 nM (3.2 nM for ATTO488-modified rectangles) using the nanophotometer. The samples were analyzed on 2% Electran® Agarose gels (DNA Grade, VWR) in 1× TAE with 11 mM $MgCl_2$ and visualized using 0.25× SYBR™

Gold stain (Invitrogen). Electrophoresis was performed using a PerfectBlue™ Gelsystem Mini M (VWR) and a PerfectBlue™ power supply (VWR) at 8.18 V cm^{-1} for 1 h with 1× TAE containing 11 mM $MgCl_2$ as the running buffer. For post-staining, the gel was incubated in 50 mL of 1× TAE containing 11 mM $MgCl_2$ and 1× SYBR™ Gold stain for 20 minutes.

For native PAGE, staple strands of the 6HB were recovered after initial folding and recycling step 10 and analyzed on a 7.5% self-cast 1.5 mm gel (29 : 1 acrylamide : bisacrylamide 40% stock solution, Himedia) using 1× TBE buffer (Carl Roth), 0.1% APS (Sigma) and 0.1% TEMED (Sigma). The samples were prepared at a total staple concentration of 5 nM, combined with 1× Orange Dye (Thermo Fisher Scientific). PAGE was performed at 100 V (PerfectBlue™ power supply, VWR) for 45 minutes (Biorad Mini-PROTEAN Tetra Cell System). Subsequently, the gel was post-stained in 1× TBE with 1× SYBR™ Gold stain for 15 minutes.

The gels were imaged using a GelJet Imager (Intas), and the bands quantified with GelAnalyzer 23.1.1 (available at **https://www.gelanalyzer.com**) by Istvan Lazar Jr., PhD and Istvan Lazar Sr., PhD, CSc.

AFM imaging

100 μL of 1 nM DON rectangles in 1× TAE with 10 mM $MgCl_2$ were adsorbed onto freshly cleaved PELCRO® mica sheets (Ted Pella, Inc) for 5 minutes. The immobilized DONs were gently washed with 15 mL of HPLC-grade water (Roth) and dried under a stream of argon. To assess SAv binding to biotinylated rectangles, 100 μL of 1× TAE with 10 mM $MgCl_2$ was added to the mica substrate, followed by 4.5 μL of 5 μM SAv (Sigma-Aldrich). After 30 minutes of incubation, the mica surface was washed with HPLC-grade water, and an additional 100 μL of 1× TAE with 10 mM $MgCl_2$ was added and incubated for 5 minutes. The sample was washed again with HPLC-grade water and dried under argon. AFM imaging was performed in air using a JPK Nanowizard Ultra Speed (JPK Instruments) operated in intermittent contact mode with HQ:NSC18/Al BS cantilevers (75 kHz, 2.8 N m^{-1}) from MikroMasch (NanoAndMore) and in ScanAsyst PeakForce Tapping mode using a Bruker Dimension ICON and SCANASYST-AIR cantilevers (70 kHz, 0.4 N m^{-1}) from Bruker. SAv binding yields were determined by manual counting, whereas the integrity of the DON rectangles was assessed by performing a particle analysis in Gwyddion[41] as described previously.[42]

Author contributions

Emilia Tomm: formal analysis, investigation, methodology, validation, visualization, writing – original draft, writing – review and editing; Guido Grundmeier: resources, writing – review and editing, supervision; Adrian Keller: conceptualization, funding acquisition, methodology, writing – review and editing, supervision.

Conflicts of interest

There are no conflicts to declare.

Data availability

Data for this article, *i.e.*, raw AFM images, are available at Zenodo at **https://doi.org/10.5281/zenodo.15147607**.

Acknowledgements

We thank B. K. Pothineni for experimental support. This work has received funding from the European Union's EIC Pathfinder Challenges 2022 programme under grant agreement No. 101115317 (NEO).

References

1 P. W. K. Rothemund, Folding DNA to create nanoscale shapes and patterns, *Nature*, 2006, **440**, 297–302.
2 S. M. Douglas, H. Dietz, T. Liedl, B. Högberg, F. Graf and W. M. Shih, Self-assembly of DNA into nanoscale three-dimensional shapes, *Nature*, 2009, **459**, 414–418.
3 D. Selnihhin, S. M. Sparvath, S. Preus, V. Birkedal and E. S. Andersen, Multifluorophore DNA Origami Beacon as a Biosensing Platform, *ACS Nano*, 2018, **12**, 5699–5708.
4 F. Nicoli, A. Barth, W. Bae, F. Neukirchinger, A. H. Crevenna, D. C. Lamb and T. Liedl, Directional Photonic Wire Mediated by Homo-Förster Resonance Energy Transfer on a DNA Origami Platform, *ACS Nano*, 2017, **11**, 11264–11272.
5 Y. Choi, L. Kotthoff, L. Olejko, U. Resch-Genger and I. Bald, DNA Origami-Based Förster Resonance Energy-Transfer Nanoarrays and Their Application as Ratiometric Sensors, *ACS Appl. Mater. Interfaces*, 2018, **10**, 23295–23302.
6 C. Steinhauer, R. Jungmann, T. L. Sobey, F. C. Simmel and P. Tinnefeld, DNA origami as a nanoscopic ruler for super-resolution microscopy, *Angew. Chem., Int. Ed.*, 2009, **48**, 8870–8873.
7 S. Pal, Z. Deng, B. Ding, H. Yan and Y. Liu, DNA-origami-directed self-assembly of discrete silver-nanoparticle architectures, *Angew. Chem., Int. Ed.*, 2010, **49**, 2700–2704.
8 B. Ding, Z. Deng, H. Yan, S. Cabrini, R. N. Zuckermann and J. Bokor, Gold nanoparticle self-similar chain structure organized by DNA origami, *J. Am. Chem. Soc.*, 2010, **132**, 3248–3249.
9 C. Zhao, X. Jiang, M. Wang, S. Gui, X. Yan, Y. Dong and D. Liu, Constructing protein-functionalized DNA origami nanodevices for biological applications, *Nanoscale*, 2024, **17**, 142–157.
10 Y. Sakai, M. S. Islam, M. Adamiak, S. C.-C. Shiu, J. A. Tanner and J. G. Heddle, DNA Aptamers for the Functionalisation of DNA Origami Nanostructures, *Genes*, 2018, **9**, 571.

11 N. Navarro, A. Aviñó, Ò. Domènech, J. H. Borrell, R. Eritja and C. Fàbrega, Defined covalent attachment of three cancer drugs to DNA origami increases cytotoxicity at nanomolar concentration, *Nanomedicine*, 2024, **55**, 102722.
12 K. Paloja, J. Weiden, J. Hellmeier, A. S. Eklund, S. C. M. Reinhardt, I. A. Parish, R. Jungmann and M. M. C. Bastings, Balancing the Nanoscale Organization in Multivalent Materials for Functional Inhibition of the Programmed Death-1 Immune Checkpoint, *ACS Nano*, 2024, **18**, 1381–1395.
13 C. Kielar, F. V. Reddavide, S. Tubbenhauer, M. Cui, X. Xu, G. Grundmeier, Y. Zhang and A. Keller, Pharmacophore Nanoarrays on DNA Origami Substrates as a Single-Molecule Assay for Fragment-Based Drug Discovery, *Angew. Chem., Int. Ed.*, 2018, **57**, 14873–14877.
14 J. Huang, A. Suma, M. Cui, G. Grundmeier, V. Carnevale, Y. Zhang, C. Kielar and A. Keller, Arranging Small Molecules with Subnanometer Precision on DNA Origami Substrates for the Single–Molecule Investigation of Protein–Ligand Interactions, *Small Struct.*, 2020, **1**, 2000038.
15 B. R. Aryal, D. R. Ranasinghe, T. R. Westover, D. G. Calvopiña, R. C. Davis, J. N. Harb and A. T. Woolley, DNA origami mediated electrically connected metal—semiconductor junctions, *Nano Res.*, 2020, **13**, 1419–1426.
16 C. Pang, B. T. Karlinsey, M. Ward, R. G. Harrison, R. C. Davis and A. T. Woolley, DNA-Templated Nanofabrication of CdS-Au Nanoscale Schottky Contacts and Electrical Characterization, *Langmuir*, 2024, **40**, 14076–14085.
17 J. L. T. Wah, C. David, S. Rudiuk, D. Baigl and A. Estevez-Torres, Observing and Controlling the Folding Pathway of DNA Origami at the Nanoscale, *ACS Nano*, 2016, **10**, 1978–1987.
18 M. DeLuca, D. Duke, T. Ye, M. Poirier, Y. Ke, C. Castro and G. Arya, Mechanism of DNA origami folding elucidated by mesoscopic simulations, *Nat. Commun.*, 2024, **15**, 3015.
19 M. Wilchek and E. A. Bayer, The avidin-biotin complex in bioanalytical applications, *Anal. Biochem.*, 1988, **171**, 1–32.
20 A.-P. Eskelinen, A. Kuzyk, T. K. Kaltiaisenaho, M. Y. Timmermans, A. G. Nasibulin, E. I. Kauppinen and P. Törmä, Assembly of single-walled carbon nanotubes on DNA-origami templates through streptavidin-biotin interaction, *Small*, 2011, **7**, 746–750.
21 H. Bui, C. Onodera, C. Kidwell, Y. Tan, E. Graugnard, W. Kuang, J. Lee, W. B. Knowlton, B. Yurke and W. L. Hughes, Programmable periodicity of quantum dot arrays with DNA origami nanotubes, *Nano Lett.*, 2010, **10**, 3367–3372.
22 I. Mela, P. P. Vallejo-Ramirez, S. Makarchuk, G. Christie, D. Bailey, R. M. Henderson, H. Sugiyama, M. Endo and C. F. Kaminski, DNA Nanostructures for Targeted Antimicrobial Delivery, *Angew. Chem., Int. Ed.*, 2020, **59**, 12698–12702.
23 C. Jiang, R. Tan, W. Li, Y. Zhang and H. Liu, Subtraction-based DNA Origami Cryptography by using Structural Defects for Information Encryption, *Small*, 2024, **20**, e2406470.
24 Y. Zhang, X. Yin, C. Cui, K. He, F. Wang, J. Chao, T. Li, X. Zuo, A. Li, L. Wang, N. Wang, X. Bo and C. Fan, Prime factorization via localized tile assembly in a DNA origami framework, *Sci. Adv.*, 2023, **9**, eadf8263.
25 N. Y. Wong, H. Xing, L. H. Tan and Y. Lu, Nano-encrypted Morse code: a versatile approach to programmable and reversible nanoscale assembly and disassembly, *J. Am. Chem. Soc.*, 2013, **135**, 2931–2934.
26 K. Busuttil, A. Rotaru, M. Dong, F. Besenbacher and K. V. Gothelf, Transfer of a protein pattern from self-assembled DNA origami to a functionalized substrate, *Chem. Commun.*, 2013, **49**, 1927–1929.
27 A. Kuzuya, M. Kimura, K. Numajiri, N. Koshi, T. Ohnishi, F. Okada and M. Komiyama, Precisely programmed and robust 2D streptavidin nanoarrays by using periodical nanometer-scale wells embedded in DNA origami assembly, *ChemBioChem*, 2009, **10**, 1811–1815.
28 N. V. Voigt, T. Tørring, A. Rotaru, M. F. Jacobsen, J. B. Ravnsbaek, R. Subramani, W. Mamdouh, J. Kjems, A. Mokhir, F. Besenbacher and K. V. Gothelf, Single-molecule chemical reactions on DNA origami, *Nat. Nanotechnol.*, 2010, **5**, 200–203.
29 J. Rackwitz, J. Kopyra, I. Dąbkowska, K. Ebel, M. L. Ranković, A. R. Milosavljević and I. Bald, Sensitizing DNA Towards Low-Energy Electrons with 2-Fluoroadenine, *Angew. Chem., Int. Ed.*, 2016, **55**, 10248–10252.
30 M. J. Neuhoff, Y. Wang, N. J. Vantangoli, M. G. Poirier, C. E. Castro and W. G. Pfeifer, Recycling Materials for Sustainable DNA Origami Manufacturing, *Nano Lett.*, 2024, **24**, 12080–12087.
31 G. Isinelli, C. M. Wintersinger, M. Aquilina, P. Lill, O. J. Young, J. Deng, W. M. Shih and Y. C. Zeng, Reusing excess staple oligonucleotides for economical production of DNA origami, *Nucleic Acids Res.*, 2025, **53**, gkaf527.
32 K. Neyra, H. R. Everson and D. Mathur, Dominant Analytical Techniques in DNA Nanotechnology for Various Applications, *Anal. Chem.*, 2024, **96**, 3687–3697.
33 E. Stahl, T. G. Martin, F. Praetorius and H. Dietz, Facile and scalable preparation of pure and dense DNA origami solutions, *Angew. Chem., Int. Ed.*, 2014, **53**, 12735–12740.
34 A. Shaw, E. Benson and B. Högberg, Purification of functionalized DNA origami nanostructures, *ACS Nano*, 2015, **9**, 4968–4975.
35 K. F. Wagenbauer, F. A. S. Engelhardt, E. Stahl, V. K. Hechtl, P. Stömmer, F. Seebacher, L. Meregalli, P. Ketterer, T. Gerling and H. Dietz, How We Make DNA Origami, *ChemBioChem*, 2017, **18**, 1873–1885.
36 J. A. Johnson, V. Kolliopoulos and C. E. Castro, Co-self-assembly of multiple DNA origami nanostructures in a single pot, *Chem. Commun.*, 2021, **57**, 4795–4798.
37 A. Ebrahimimojarad, Z. Wang, Q. Zhang, A. Shah, J. S. Brenner and J. Fu, A Robust and Efficient Method to Purify DNA-Scaffolded Nanostructures by Gravity-Driven

Size Exclusion Chromatography, *Langmuir*, 2024, **40**, 8365–8372.

38 Y. Xin, P. Piskunen, A. Suma, C. Li, H. Ijäs, S. Ojasalo, I. Seitz, M. A. Kostiainen, G. Grundmeier, V. Linko and A. Keller, Environment-Dependent Stability and Mechanical Properties of DNA Origami Six-Helix Bundles with Different Crossover Spacings, *Small*, 2022, **18**, e2107393.

39 C. Chau, G. Mohanan, I. Macaulay, P. Actis and C. Wälti, Automated Purification of DNA Origami with SPRI Beads, *Small*, 2024, **20**, e2308776.

40 S. Fan, D. Wang, J. Cheng, Y. Liu, T. Luo, D. Cui, Y. Ke and J. Song, Information Coding in a Reconfigurable DNA Origami Domino Array, *Angew. Chem., Int. Ed.*, 2020, **59**, 12991–12997.

41 D. Nečas and P. Klapetek, Gwyddion: an open-source software for SPM data analysis, *Open Phys.*, 2012, **10**, 181–188.

42 M. Hanke, D. Dornbusch, E. Tomm, G. Grundmeier, K. Fahmy and A. Keller, Superstructure-dependent stability of DNA origami nanostructures in the presence of chaotropic denaturants, *Nanoscale*, 2023, **15**, 16590–16600.